Journal of Sound and Vibration (1997) **206**(2), 169–194

A COMPUTATIONAL STUDY OF CONTOURED PLUG-NOZZLE JET NOISE

I. S. Das

The Pennsylvania State University, *Sharon*, *Pennsylvania* 16146, *U.S.A.*

A. Khavaran

Lewis Research Center Group, *NYMA*, *Cleveland*, *Ohio* 44135, *U.S.A.*

AND

E. A. Krejsa

NASA Lewis Research Center, *Cleveland*, *Ohio* 44135, *U.S.A.*

(*Received* 11 *March* 1996, *and in final form* 14 *March* 1997)

A computational noise study of a scale model of an axisymmetric ideally contoured plug-nozzle (CPN) is presented. The CPN has an exit diameter of 45 mm and the geometrical configuration is such that the jet flow is shockless at the design pressure ratio, $\xi_d = 3{\cdot}62$. The gas dynamics of the jet flows has been predicted using the NPARC Computational Fluid Dynamics code with the k-ε turbulence model. The gas dynamics data are then used to perform the noise computations based on the modified General Electric MGB code. The study covers a range of pressure ratios, $2{\cdot}0 \leqslant \xi \leqslant 5{\cdot}0$. The agreement of the computational aeroacoustic results with the reported experimental data is favorable. At the design pressure ratio (shockless flow), the predicted noise levels are within 3 dB. At the off-design pressure ratios (flows with shocks), the theory predicts the noise levels within 5 dB, except at very high frequencies for pressure ratios farthest from the design pressure ratio when deviations up to 8 dB are noted. The computed directivity patterns do not represent the reported experimental trends well. The mechanism of shock formation in the CPN jet flows is noted to be basically different from those in the convergent nozzle and convergent–divergent nozzle jet flows. The computational results indicate consistent noise reduction effectiveness of the CPN relative to the equivalent convergent and convergent–divergent nozzles for all operating pressure ratios.

1. INTRODUCTION

The need to develop a high speed cruise aircraft has lately been felt by the commercial aircraft industry which means that the problem of supersonic jet noise suppression must be addressed. The magnitude of the challenge can be appreciated by noting that the four Olympus engines of the Concorde produce noise levels of 12, 18, and 13 EPNdB above the Federal Aviation Administration FAR 36 Stage III noise regulations for sideline, cutback and approach, respectively. Earlier jet noise suppression efforts could achieve noise reductions of the order of only 2 EPNdB per percent thrust loss, whereas the FAR Stage III regulations would require a noise reduction of the order of 4 EPNdB per percent thrust loss [1, 2].

In perfectly expanded (shock-free) supersonic jet flows, the noise mechanism is primarily due to turbulent mixing which depends upon the mean flow speed, the flow velocity gradients downstream of the nozzle exit, and the turbulence characteristics [3]. Imperfectly

0022–460X/97/370169 + 26 $25.00/0/sv971038

expanded supersonic jet flows contain repetitive shocks which interact with turbulence related fluctuations generating: (a) harmonically related discrete tones of noise often termed ''screech'' [4], and (b) broadband but strongly peaked shock-associated noise [5–9]. The shock structure and its interaction with the convecting turbulence structure may also change the turbulence structure which then affects the strength of the mixing noise sources. It is generally recognized that shock-associated noise is dominant at off-design supercritical pressure ratios, at lower temperatures and at higher angles to the downstream jet axis. The intensity of shock-associated noise is known to be dependent upon (1) the strength and the spacing of the repetitive shock cells, and (2) the strength and coherence of the flow fluctuations convected through the shock fronts. Therefore, to suppress the dominant shock-related noise component, the characteristics of the shock structure need to be modified such that the contributing noise sources and the effectiveness of their noise generating mechanism are both reduced.

Use of a contoured convergent–divergent (CD) nozzle is often considered a design option for attenuating the shock-associated noise component generated by the exhaust flow of modern high specific thrust jet engines. The shock-associated noise component is eliminated if the exhaust flow of a contoured CD nozzle, operated at its design pressure ratio, is shock free. However, in practice, such exhaust nozzles are operated over an extended range of pressure ratios, where at the off-design pressure ratios in either the over- or the underexpanded mode, the repetitive shock structure is formed in the exhaust flows. At low supercritical pressure ratios, the shock structure may even be present in the diverging part of the contoured CD nozzle. The overall sound pressure level as a function of the fully expanded jet Mach number M_j of the moderately over- and underexpanded CD nozzle jet has been shown to be significantly lower than those of an equivalent (i.e., of the same mass flow rate, operating pressure ratio, and the exhaust area) round convergent nozzle [5, 10].

Some recent experimental acoustic studies of supersonic jet flows from plug-nozzles have also shown appreciable shock noise suppression effects [11–15]. In some of these plug-nozzle studies, the plugs were rather long cylindrical center bodies [11, 12] and in others [13, 14] the plug surface was uncontoured with pointed or truncated termination. A repetitive cellular shock structure is necessarily formed in the supersonic jet flows from such nozzles. Moreover, long plugs are likely to have related aerodynamic and weight penalties. Therefore, to circumvent some of these disadvantages and to eliminate or to weaken the repetitive shock structure in supersonic jet flows, using a short contoured externally expanded plug with a pointed termination suggests itself as an attractive alternative. The plug surface of such a *minimum length* supersonic plug-nozzle cancels all of the incident expansion waves, and the exhaust flow is shockless at the design condition. Preliminary experimental noise study of an ideal *contoured* plug-nozzle with a *pointed* termination (CPN) [15] reported substantial reductions in the noise levels relative to an equivalent convergent nozzle; these reductions were noted at all observation angles and at all off-design and design pressure ratios. The CPN jet flows were found to considerably inhibit the growth and the strength of shock structures when operated at off-design supercritical pressure ratios, thereby reducing the intensity of the shock-associated noise component. The noise suppression effectiveness of the CPN was observed to be of the same order as that of an equivalent contoured CD nozzle at the same design pressure ratio (shockless flows). But, at the off-design pressure ratios (flows with shocks), the noise suppression effectiveness of the CPN was reported to be better than that of the equivalent CD nozzle. It is thus clear that the presence of a suitable plug results in significant jet noise suppression through weakening/elimination of repetitive shock cells.

A simple single stream plug-nozzle on its own may not be able to meet the demands of the FAR 36 Stage III noise regulations. However, a plug of suitable geometry could be accommodated inside single- or multistream nozzle schemes such as co-axial nozzles [16, 17], rectangular geometry supersonic nozzles [18], elliptical geometry supersonic nozzles [19, 20] and ejector–mixer nozzles [21] which have been considered recently for supersonic jet noise suppression. Placement of suitable plug(s) could add to the noise suppression effectiveness of these nozzles without plugs.

Evaluating the role of an ideally contoured plug in a supersonic jet is an important step towards use of suitable plug(s) in future nozzle schemes to achieve satisfactory jet noise suppression. The only reported study of a contoured plug-nozzle jet noise is a preliminary experimental investigation [15] which focused largely upon the far-field noise measurements, and no flow field measurements other than the shadowgraph records are available. The aim of the present theoretical study is to estimate the gas dynamics and the far-field noise characteristics of the jet flows of an ideal CPN in the over-, the fully-, and the underexpanded modes of operation over a range of supercritical pressure ratios appropriate for practical jet engine applications. In the shock-free and virtually wakeless supersonic jet flow issuing from a CPN operating at its design pressure ratio, the noise generating mechanism is primarily due to turbulent mixing. The far-field computational acoustic data of shockless supersonic jet flows of such a plug-nozzle also serve as the baseline acoustic spectral data for a comparative computational assessment of (1) the shock-associated noise when the CPN is operated at off-design conditions, and (2) the noise suppression effectiveness of the improperly expanded supersonic jet flows issuing from equivalent plug-nozzles of other geometry, configuration and termination.

2. CONTOURED PLUG-NOZZLE JET FLOW

A fully external-expansion contoured plug-nozzle (CPN) is a modification of a conventional CD nozzle. It combines a convergent nozzle and a contoured plug, where the supersonic expansion downstream of the sonic throat of the covergent nozzle occurs externally over the plug surface. Unlike the CD nozzle, the CPN jet flow in part is controlled by the ambient back pressure and not by the nozzle wall. Therefore, the free jet boundary downstream of the CPN throat is self-adjusting. At the design pressure ratio, the CPN jet flow at the exit is uniform, axial, and shockless (see Figure 1). The design of the isentropic plug profile for an axially symmetric, full external expansion CPN is based on the following key considerations.

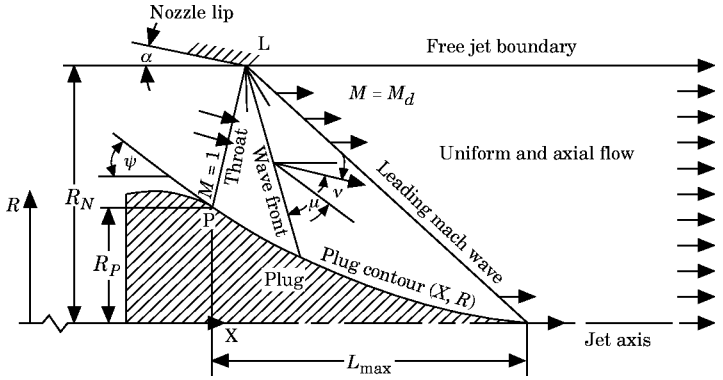

Figure 1. Fully expanded jet flow from an ideal contoured plug-nozzle; $LP = W_t$, $K = R_P/R_N$.

The expansion waves are assumed to be centered at the nozzle lip L (Figure 1). In the expansion over the shoulder of an axially symmetric body, the flow in the limit is given by the two-dimensional Prandtl–Meyer theory. Therefore, for the free jet flow boundary at the lip to be straight and parallel to the nozzle axis, the converging lip has to have an inclination α, which must be equal and opposite to the Prandtl–Meyer angle v for the design Mach number M_d.

The expansion waves emanating as a fan centered at the nozzle lip and incident on the plug surface are all canceled by suitable compression turns provided at the plug surface. The leading expansion wave of the fan (corresponding to M_d) must end at the plug tip and is straight, being the start of the uniform flow region. The plug contour is a streamline of the potential (isentropic) flow issuing from the plug-nozzle. A methodology for designing an isentropic supersonic inlet plug using the method of characteristics was developed by Connors and Meyer [22]. Their method assumed a straight sonic line, a finite plug-tip angle and a finite strength oblique shock extending from plug tip to nozzle lip. Plug contours were predicted for relatively high design pressure ratios. It was suggested that this approach for the inlet plug design would also be applicable to the prediction of the plug contour of an externally expanded ideally contoured plug-nozzle. For an ideally contoured plug-nozzle of a given convergent lip radius R_N, the maximum length of the contoured plug L_{max} and the annulus radius ratio K (ratio of the plug radius at the sonic point to the radius of the nozzle lip) are unique functions of M_d [23]. At a high design pressure ratio (i.e., high M_d), the value of K is large which results in a small annulus width of the throat W_t. Therefore, the assumption of a straight sonic line is reasonably satisfied at high design pressure ratios. The present study, however, focuses on plug-nozzles of lower design pressure ratios normally encountered in turbojet engines for supersonic jet propulsion. This range of low pressure ratios was not covered in the earlier prediction of contours of inlet plugs [22]. At lower design pressure ratios, ξ_d, the annulus radius ratio, K, of the plug-nozzle is smaller and, therefore, the annulus width, W_t, is comparatively larger. Also, because of considerable differences in the slopes of the inner and outer walls at the throat, the flow at the throat is essentially non-uniform. The sonic line would thus have an appreciable curvature under such conditions. Consequently, an exact prediction of the curved sonic line is necessary for obtaining the isentropic plug profile of a minimum length contoured plug-nozzle.

The design parameters that must be determined for the start of a numerical solution scheme are the annulus radius ratio, K, the outer wall (lip) slope, α, the inner wall (plug) slope at the sonic point, ψ, the maximum plug length, L_{max} and the exact shape of the sonic line. These parameters were estimated for a design Mach number $M_d = 1{\cdot}5$ in the earlier study [15]. A plug having an ideal contour (pointed tip and isentropic profile) may not be a practical choice. In such cases, the geometry of a non-contoured plug should closely agree with the overall geometry of the ideally contoured plug in order to achieve the maximum possible noise reduction benefit through the use of a plug. A set of charts showing the functional dependence of the overall geometric parameters K, α, ψ and L_{max} on the design Mach number, M_d, is provided in reference [24].

3. PLUG-NOZZLE CONFIGURATION

The computational gas dynamics/noise study is for a contoured plug-nozzle geometry of the Syracuse experimental study [15]. This permits a comparison of the predicted gas dynamics/noise data with the measurements. A complete geometry of the annular flow boundaries (plug-stem surface is the inner boundary and inner nozzle surface is the outer boundary) is presented in Table 1. The reference point ($X = 0$, $R = 0$) is located on the

TABLE 1

Co-ordinates of the contoured plug and converging nozzle surfaces

X-Plug	*R*-Plug	*X*-Noz	*R*-Noz	*X*-Plug	*R*-Plug	*X*-Noz	*R*-Noz
0	0·955	0	15·24	10·5697	0·955	9·0882	7·03
0·2072	0·955	0·1782	15·238	10·777	0·955	9·2664	6·8042
0·4145	0·955	0·3564	15·2319	10·9842	0·955	9·4446	6·589
0·6217	0·955	0·5346	15·2218	11·1915	0·955	9·6228	6·3836
0·829	0·955	0·7128	15·2076	11·3987	0·955	9·801	6·1873
1·0362	0·955	0·891	15·1893	11·606	0·955	9·9792	5·9994
1·2435	0·955	1·0692	15·1669	11·8132	0·955	10·1574	5·8193
1·4507	0·955	1·2474	15·1404	12·0205	0·955	10·3356	5·6466
1·658	0·955	1·4256	15·1096	12·2277	0·9624	10·5138	5·4809
1·8652	0·955	1·6038	15·0746	12·435	0·9869	10·692	5·3217
2·0725	0·955	1·782	15·0353	12·6422	1·029	10·8702	5·1687
2·2797	0·955	1·9602	14·9916	12·8495	1·0897	11·0484	5·0216
2·487	0·955	2·1384	14·9435	13·0567	1·2033	11·2266	4·8802
2·6942	0·955	2·3166	14·8909	13·264	1·2835	11·4048	4·7442
2·9015	0·955	2·4948	14·8336	13·4712	1·3536	11·583	4·6133
3·1087	0·955	2·673	14·7715	13·6785	1·4139	11·7612	4·4874
3·316	0·955	2·8512	14·7046	13·8857	1·4649	11·9394	4·3662
3·5232	0·955	3·0294	14·6327	14·093	1·5067	12·1176	4·2496
3·7305	0·955	3·2076	14·5557	14·3002	1·5397	12·2958	4·1375
3·9377	0·955	3·3858	14·4734	14·5075	1·564	12·474	4·0297
4·145	0·955	3·564	14·3855	14·7147	1·5797	12·6522	3·926
4·3522	0·955	3·7422	14·292	14·922	1·5869	12·8304	3·8264
4·5595	0·955	3·9204	14·1925	15·1292	1·5856	13·0086	3·7307
4·7667	0·955	4·0986	14·0868	15·3365	1·5759	13·1868	3·6388
4·974	0·955	4·2768	13·9746	15·5437	1·5576	13·365	3·5506
5·1812	0·955	4·455	13·8555	15·751	1·5308	13·5432	3·4661
5·3885	0·955	4·6332	13·7293	15·9582	1·4952	13·7214	3·3851
5·5957	0·955	4·8114	13·5953	16·1655	1·4506	13·8996	3·3076
5·803	0·955	4·9896	13·4532	16·3727	1·3969	14·0778	3·2335
6·0102	0·955	5·1678	13·3023	16·58	1·3337	14·256	3·1627
6·2175	0·955	5·346	13·1419	16·7872	1·2606	14·4342	3·0952
6·4247	0·955	5·5242	12·9713	16·9944	1·1772	14·6124	3·0309
6·632	0·955	5·7024	12·7895	17·2017	1·0829	14·7906	2·9697
6·8392	0·955	5·8806	12·5952	17·4089	0·977	14·9688	2·9116
7·0465	0·955	6·0588	12·3871	17·409	0·977	15·147	2·8566
7·2537	0·955	6·237	12·1633	17·609	0·87	15·3252	2·8046
7·461	0·955	6·4152	11·9215	17·819	0·759	15·5034	2·7556
7·6682	0·955	6·5934	11·6586	18·029	0·646	15·6816	2·7095
7·8755	0·955	6·7716	11·3706	18·209	0·569	15·8598	2·6664
8·0827	0·955	6·9498	11·0515	18·389	0·489	16·038	2·626
8·29	0·955	7·128	10·6923	18·569	0·417	16·2162	2·5882
8·4972	0·955	7·3062	10·2781	18·764	0·345	16·3944	2·5506
8·7045	0·955	7·4844	9·8212	18·959	0·28	16·5726	2·513
8·9117	0·955	7·6626	9·4064	19·214	0·202	16·7507	2·4755
9·119	0·955	7·8408	9·0299	19·439	0·14	16·9289	2·4379
9·3262	0·955	8·019	8·6838	19·604	0·099	17·1071	2·4003
9·5335	0·955	8·1972	8·363	19·776	0·064	17·2853	2·3628
9·7407	0·955	8·3754	8·0636	20·03	0·025	17·4635	2·2352
9·948	0·955	8·5536	7·7827	20·234	0·005	17·6417	2·2876
10·1552	0·955	8·7318	7·5179	20·335	0·00001		
10·3625	0·955	8·91	7·2675				

jet axis (an axis of symmetry) at the start of the converging section of the nozzle; the X-axis is directed along the downstream jet axis, and the radial R-axis is perpendicular to the jet axis. The nominal design Mach number of this plug-nozzle is 1·5. The corresponding overall geometrical parameters annulus radius ratio, K, the lip angle, α, the plug-surface angle at the sonic point, Ψ, and ratio of the maximum length to the lip radius, (L_{max}/R_n), are, respectively, 0·43, 11·91°, 28·4° and 1·30. The plug-nozzle has a lip of radius $R_n = 22{\cdot}5$ mm and a lip thickness of 0·25 mm. The ratio of the converging nozzle inlet to exit area is 46. It was reported that the plug-nozzle jet was shockless at the design pressure ratio of $\xi_d = 3{\cdot}62$ and jet screech noise was noted to be absent. For further details of the experimental setup, see reference [15].

4. METHOD OF SOLUTION

It is generally accepted that the direct numerical simulation based on the full, unsteady, compressible Navier–Stokes equations governs both the generation and the propagation of sound. Current efforts in this area of study, usually labeled as computational aeroacoustics, are directed towards resolving various computational issues, such as grid resolution for frequencies of interest, computational domain, boundary conditions, finite difference scheme, shock noise formulation and so on. A unified aerodynamic/acoustic code (the MGB code) was developed at General Electric [25]. In the GE methodology, the aerodynamic predictions were carried out by applying an extension of Reichardt's model [26]. The components of turbulent shear stress are computed based upon contour integrals around the nozzle exit geometry and utilized in deriving an expression for the source strength. Reichardt's solution neglects the radial mean flow and swirl, and the effect of shock structure, if present, on mixing and turbulence. The closed-form nature of this solution results in a relatively fast numerical scheme, but the predictions for complex geometry are found to be unsatisfactory. The methodology was subsequently modified by NASA Lewis researchers [27, 28] applying a two-stage algorithm. Reichardt's model was replaced by a CFD Navier–Stokes solver and the aerodynamic calculations were carried out independently. The resulting plume data were then used for noise computation. The two-stage algorithm has the following advantages: (1) start of the aerodynamics calculations from within the nozzle giving a more realistic model of exit conditions, (2) independent grid selection for aerodynamic and acoustic purposes, and (3) proper prediction of shock-cell structure as well as shock intensity essential for prediction of the shock-associated noise. For full details of the NASA Lewis methodology, see references [27] and [28].

The flow field computation in the present study is based on the axisymmetric version of the NPARC code [29] with Chien's k-ε turbulence model [30]. This CFD code is an evolution of the PARC code developed by the Arnold Engineering Development Center, which in turn was based upon the NASA Ames ARC code. This extensively validated code solves the complete Reynolds-averaged Navier–Stokes equations in conservative law form. The Beam and Warming approximate factorization algorithm [31] is used for forming the implicit central difference scheme. The viscous coefficients are determined based on Sutherland's law, Stokes's hypothesis, and constant Prandtl number assumptions. A Baldwin and Lomax type turbulence model [32] is utilized to compute the boundary values and initial conditions for k and ε.

The solution technique for noise prediction in the present study is based upon the NASA Lewis methodology. In what follows, only an overview of the methodology is presented. The first section briefly describes the application of the NPARC code with k-ε turbulence model for computation of the source strength and its spectrum, and explains the empirical

constants used in the computation of the characteristic Strouhal number and the supersonic convection factor. In the second section, the effect of the surrounding medium (velocities and temperature gradients) on the noise radiated from the convecting quadrupole sources is discussed. The third section presents an outline of the shock-associated noise prediction scheme.

4.1. SOURCE SPECTRUM MODEL

It is generally recognized that at subsonic and low supersonic speeds, small scale turbulence is the primary source of mixing noise. Each finite volume of turbulence may be described as a multipole source that convects downstream and emits sound that is refracted by mean flow gradients. As the jet becomes highly supersonic, large-scale structures or instability waves of the flow become increasingly active. The prediction scheme assumes the dominance of fine-scale turbulence. In a fine-scale turbulence, it is assumed that the turbulence length scale is small. Lilley's equation suggests that, at subsonic convection Mach numbers, the radiation field arriving from each source volume element is independent of that due to any other region of the flow. As such, the mean square pressure at any point in the sound field is simply the sum of the mean square pressures produced by independent correlation volume elements that make up the jet. The compactness condition is not that restrictive and may hold true even at moderate supersonic Mach numbers. With the compact eddy approximation, the solution is expressed as a Fourier transform of the space-time correlation function to be integrated over the entire jet volume. This requires modelling of the space-time correlation function.

Following Lighthill's acoustic analogy approach, the mean square acoustic pressure in the far-field in the absence of convection and refraction may be written as

$$\overline{p^2}(R, \theta, \phi) = \frac{R_i R_j R_k R_l}{16\pi^2 C_\infty^4 R^6} \int_{\vec{y}} \int_{\vec{\xi}} \frac{\partial^4}{\partial \tau^4} \overline{(T_{ij} T'_{kl})}\, \mathrm{d}\vec{\xi}\, \mathrm{d}\vec{y}. \tag{1}$$

The source strength is assumed to be dominated by the unsteady momentum flux, i.e., $T_{ij} \sim \rho V_i V_j$. The vector $\vec{\xi}$ is the separation vector between locations $\vec{y}$ and $\vec{y} + \vec{\xi}$ having correlations $\rho V_i V_j$, and $\rho' V'_k V'_l$, respectively, and τ is the time delay of correlation. The corresponding spectrum, in terms of the Fourier transform of the autocorrelation function, is

$$\overline{p_\omega^2} = \frac{1}{2\pi} \int_{-\infty}^{\infty} \overline{p^2}\, \mathrm{e}^{\mathrm{i}\omega\tau}\, \mathrm{d}\tau. \tag{2}$$

As such, for a quasi-incompressible turbulence, the source strength is characterized by a two-point time-delayed fourth order velocity correlation tensor. For a nearly parallel mean flow, contributions of the self-noise terms may be shown to be independent of the mean flow. Assuming a normal joint probability for turbulent velocity components and following Batchelor's model for isotropic turbulence, the fourth order correlation is a linear combination of the second order correlations,

$$\overline{v_i v_j v'_k v'_l} = \overline{(v_i v'_k)}\,\overline{(v_j v'_l)} + \overline{(v_i v'_l)}\,\overline{(v_j v'_k)} + \overline{(v_i v'_j)}\,\overline{(v_k v'_l)}. \tag{3}$$

By assuming the two-point velocity correlation to be separable in space/time factors,

$$\overline{v_i v'_j} = R_{ij}(\vec{\xi}) g(\tau), \tag{4}$$

the integration can be carried out in closed form. The space factor may be written as

$$R_{ij}(\vec{\xi}) = T[(f + \tfrac{1}{2}\xi f')\delta_{ij} - \tfrac{1}{2}f'\xi_i\xi_j/\xi], \tag{5}$$

where $T = [\overline{(v_i v_i)}/3]$ is the intensity of turbulence replacing the axial turbulence in Reichardt's model and $f' = \partial f/\partial\xi$ and $f(\xi) = \exp[-\pi\xi^2/L^2]$, L being the longitudinal macroscale of turbulence. The time factor of correlation may be expressed as $g(\tau) = \exp[-(\tau/\tau_0)^2]$, where τ_0 is the characteristic time delay in the moving reference frame. For axisymmetric jets, it has been shown that τ_0 is proportional to the inverse of mean shear. The eddy length scale L_ε is related to the kinetic energy of turbulence, $k = \overline{(v_i v_i)}/2$, and its dissipation rate ε as $L_\varepsilon = k^{3/2}/\varepsilon$. Assuming $L \sim L_\varepsilon$, it can be shown that $1/\tau_0 \sim \varepsilon/k$. Contribution to self noise due to various components of the source correlation tensor I_{ijkl} may be expressed in closed form as $I_{1111} = I_{2222} = I_{3333} = 8I_{1122} = 8I_{2233}$ and $I_{1212} = I_{1313} = I_{2323} = (7/16)I_{1111}$. Acoustic/flow interaction for an arbitrary eddy volume element is obtained by multiplying each correlation component by the corresponding directivity factor. In the final analysis, the source terms will become proportional to the term I_{1111}. The first component of source/spectrum correlation tensor is given by [25]

$$I_{1111}(\Omega) = (3/8\sqrt{\pi})\rho^2 k^{7/2}(\Omega\tau_0)^4 \exp[-(\Omega\tau_0)^2/8], \tag{6}$$

which is used to compute the noise field in conjunction with the refraction effect of the mean flow. The Doppler effect relating the source frequency Ω and the observer frequency f is given by $\Omega = 2\pi f\bar{C}$, where the eddy convection factor, $\bar{C} = (1 - M_c\cos\theta)$. In the modified computational approach, the eddy convection factor is taken as

$$\bar{C} = \sqrt{(1 - M_c\cos\theta)^2 + (\alpha_c\sqrt{k}/C_\infty)^2}. \tag{7}$$

The empirical constant α_c has been assumed to be 0·5. An average value of the convection Mach number M_c in the initial mixing region of the jet is $0{\cdot}62M_j$. Experimental measurements [33] show that the convection velocity may vary across the jet. Variation of the convection Mach number with the source location may be taken as a weighted average of the exit Mach number and the local Mach number,

$$M_c = 0{\cdot}5M + \beta_c M_j. \tag{8}$$

The convection constant β_c in the range of 0·25 to 0·3 appears to yield the best results and a value of 0·3 has been selected.

4.2. SOUND/FLOW INTERACTION

The effect of the surrounding mean flow on acoustic radiations caused by convecting multipole sources, which is not accounted for by the acoustic analogy approach, needs to be incorporated. Many investigators have studied the radiation field of multipole sources in parallel sheared flows. Mani studied the mean flow interaction of round jets for slug flow profiles assuming quadrupole sources convecting along the centerline of the jet [34]. His analysis was extended to arbitrary velocity profiles in the high frequency and low frequency limits and then generalized for arbitrarily located sources in continuously varying monotonic profiles [35, 36]. It has been proposed that the high frequency solution provides adequate approximation for supersonic jets [37, 38].

The non-linear terms in Lighthill's analysis are entirely contained in the source term $T_{ij} = (\rho + \rho')v_i v_j + \delta_{ij}(p - C_\infty^2\rho') - e_{ij}$, where ρ and ρ' denote the mean and fluctuating density, p is the acoustic pressure, C_∞ is the ambient sound speed and e_{ij} is the viscous stress tensor. This source term can be approximated as $T_{ij} \sim \rho v_i v_j$ by assuming small entropy change and neglecting e_{ij} compared with much larger Reynolds stress term $\rho v_i v_j$ [39]. In addition to quadrupole sources (proportional to ρ), a mean density gradient in heated jets may result in lower order singularities. These range from simple sources (proportional to

$d^2\rho/dr^2$ and $(1/r)\,d\rho/dr$) to dipole type sources (proportional to $d\rho/dr$), which are known to generate noise scaling to U^4 and U^6, respectively. The present work assumes that convected quadrupoles are the primary noise generators (see reference [33]).

Other variations of Lighthill's equation, such as Lilley's or Phillips' formulations have the advantage of separating fluids effects from the sound generating term. For example, in Lilley's formulation, the terms corresponding to source convection and sound refraction appear in the operator part of the equation. Apart from the added complexity, the other disadvantage of the Lilley's equation is its non-linearity. But the turbulence velocities in the jet are fairly small compared to the mean velocity (see Figure 5(b)). Hence, for many practical cases of interest, assuming that the jet is not highly supersonic, it is reasonable to neglect terms on the operator side of the equation involving the product of the fluctuating quantities and to replace the velocity and sound speed by their mean values. Physically, this linearization process amounts to ignoring effects such as scattering of sound by turbulence.

The sound/flow interaction effect consideration is primarily based on the axisymmetric solution of the Lilley's equation developed by Mani and Balsa [25]. The mean square acoustic pressure in the far field is given by

$$\overline{p^2}(R, \theta, \Omega) = \int_{\vec{y}} \Lambda(a_{xx} + 4a_{xy} + 2a_{yy} + 2a_{yz})\,d\vec{y}, \tag{9}$$

where $a_{xx}, \ldots, a_{yz}$ are the directivity factors which describe the noise field due to each of the quadrupoles contained within a turbulent eddy volume element. The weighting factors are those derived by Ribner [40]. Factor Λ, related to the source intensity and frequency, is

$$\Lambda \simeq (\rho_\infty/\rho - 1)^2 I_{1111}(\Omega)/(4\pi R C_\infty C)^2(1 - M\cos\theta)^2(1 - M_c\cos\theta)^2. \tag{10}$$

The directivity factors are functions of the shielding function g^2, given by

$$g^2(r) = [(1 - M\cos\theta)^2(C_\infty/C)^2 - (\cos\theta)^2]/(1 - M_c\cos\theta)^2. \tag{11}$$

The mean flow variables obtained from the CFD computation are used to estimate $g^2(r)$ and hence the directivity factors. The location where $g^2(r)$ changes sign is known as the turning point. A negative value of $g^2(r)$ between the source and the observer indicates the possibility of fluid shielding. The position of source with respect to the turning points of $g^2(r)$ contributes to the amount of shielding by a factor of $\exp[-2K\int_{r_1}^{r_2}\sqrt{|g^2(r)|}\,dr]$, where the limits are determined by the source location with respect to the turning points, and $K = \Omega/C_\infty$ is the wave number.

A correction of one Doppler factor has been utilized for the source volume effects [41]. The correction for flight speed has been included using the flight dynamic factor, $(1 + M_\infty\cos\theta)^{-1}$, where M_∞ is the flight number.

4.3. SHOCK-ASSOCIATED NOISE PREDICTION

The mechanism of generation of the shock-associated noise is not clearly understood and a general theoretical modelling effort has yet to reach a satisfactory stage. The distinctive features of shock-associated noise for choked convergent nozzle jet flows were identified in Harper-Bourne and Fisher's experimental study [6] and these were later confirmed by Tanna [9] for a wide range of operating conditions. It was observed that for low supersonic Mach numbers, the shock-associated noise intensity I scaled as the fourth power of a shock strength parameter $\beta = (M_j^2 - 1)^{1/2}$. For high supersonic Mach numbers, the scaling breaks down because of the Mach disc formation. By extending Powell's model

for the jet screech tones [4], Harper-Bourne and Fisher proposed a point source array model where the acoustic energy source is located at the end of each shock cell and the relative phasing between the sources is correlated by the spacing and the convection speed of the turbulent eddies between them. In a later formulation, Tam and Tanna considered that shock-associated noise is generated by weak interaction between the quasi-periodic shock cells and the downstream propagating, large scale turbulence structures in the mixing layer of the jet [10]. The Harper-Bourne and Fisher results for the choked convergent nozzle follow from the Tam and Tanna formulation for the CD nozzle when the design Mach number is set to unity. This agreement appears to be due to the fact that both models describe generation of noise by the coherent scattering of sound sources.

Tam and Tanna's shock-associated noise formulation [10] is based on Pack's vortex sheet shock cell model [42] which assumes that the mixing layer is thin and thus can be treated as a vortex sheet. This approximation is valid only close to the exit of the jet, and it breaks down as the jet spreads downstream. A later development considers a multiple scales shock cell model which accounts for spreading of the mean flow, and represents the shock cell structure by a superposition of the wave guide modes of the jet flow [43]. The mechanism is further elaborated in Tam's stochastic model theory in which the large turbulence structures are represented by a superposition of the intrinsic instability waves of the mean jet flow [44, 45]. Combined with the multiple-scales shock cell model, the stochastic model theory predicts both the near and far field spectra.

The shock-associated noise prediction methodology incorporated in the code follows the formulations of Tam and his associates. The shock-associated noise power spectral density at a point (r, θ) is given by

$$S(r, \theta, f) = \Gamma L_w^2 A_j \overline{A^2} \left(\frac{\rho_\infty^2 C_\infty^4 M_j^2}{f(fD_j/U_j)} \right) \Big/ \left(1 + \frac{\gamma - 1}{2} M_d^2 \right) r^2$$

$$\times \sum_{m=1}^{\infty} \frac{1}{\sigma_m^2 \mathrm{J}_1^2(\sigma_m)} \exp \left\{ - \left(\frac{(f_m - f)(1 + M_c \cos\theta) L_W}{f(U_c/U_j)} \right)^2 \frac{1}{2 \ln 2} \right\}, \tag{12}$$

where Γ is an unknown empirical constant and L_w is the half-width of Tam's "similarity source model" and is related to the core length of the jet. Both parameters need to be determined by fitting the prediction formula to the experimental data. The fully-expanded jet diameter D_j is related to the nozzle exit diameter D through the mass conservation equation as

$$\frac{D_j}{D} = \left[\left(1 + \frac{\gamma - 1}{2} M_j^2 \right) \Big/ \left(1 + \frac{\gamma - 1}{2} M_d^2 \right) \right]^{(\gamma + 1)/4(\gamma - 1)} \left(\frac{M_d}{M_j} \right)^{1/2}. \tag{13}$$

The parameter σ_m is the mth root of the zeroth order Bessel function and f_m is defined as

$$f_m = U_c k_m / 2\pi(1 + M_c \cos\theta), \tag{14}$$

where k_m corresponds to the wave number of the mth wave-guide mode of the shock cell structure at maximum wave amplitude. J_1 is the Bessel function of order one. The quantity $\overline{A^2}$ which characterizes the shock cell strength (to be determined semi-empirically to improve the prediction) is given by

$$\overline{A^2} = \left[\left((M_j^2 - M_d^2)\Big/\left(1 + \frac{\gamma - 1}{2} M_d^2\right)\right)^2 \left(\frac{D}{D_j}\right)^2\right] \times \left[1 + n_1 \left((M_j^2 - M_d^2)\Big/\left(1 + \frac{\gamma - 1}{2} M_d^2\right)\right)^{n_2}\right], \quad (15)$$

where $n_1 = 3{\cdot}0$, $n_2 = 3{\cdot}0$ for underexpanded flows and $n_1 = 6{\cdot}0$, $n_2 = 5{\cdot}0$ for overexpanded flows. These values in Tam's model are based upon the measurements of the convergent–divergent nozzle jet flows so that a better match between the prediction and the experimental data for such flows could be attained. It should be emphasized that the shock-noise prediction is not based upon the CFD data computed for the CPN jets.

The prediction incorporates the hot jet effect and it has been further modified to accommodate the forward flight effect [46].

5. COMPUTATIONAL DOMAIN AND SCOPE OF DATA

The axisymmetric flow field is represented by a computational domain consisting of a 151 × 351 grid (Figure 2), which is highly clustered along all the solid surfaces and along the plug-nozzle lip line in the jet exit region. The domain starts at the beginning of the converging inlet of the plug-nozzle and extends to an axial length of $33D$ and has an outer radius of $11D$ (the plug-nozzle exit diameter $D = 45$ mm and the aspect ratio = 3). That is, the domain is contained within $X = 0$, $X = 33D$ and $Y = 0$, $Y = 11D$.

The computational flow boundary conditions are as follows: all solid surfaces are assigned as no-slip, adiabatic wall conditions; all velocity components and the normal gradients of pressure and temperature are set to zero on boundary segments using this option. The jet axis downstream from the plug tip is prescribed as an *axis of symmetry*; this is very similar in function to the slip–surface boundary condition. The upper bounding surface ($Y = 11D$) of the domain is set as a slip surface; all flow gradients normal to this boundary segment along with the component of velocity normal to this surface are taken to be zero. The conditions at the inlet ($X = 0$) and the exit ($X = 33D$) are assumed to be *free stream* boundary conditions; on these external far-field boundary segments, imposition of the correct subsonic or supersonic, inflow or outflow state is taken care of automatically. The assumed ambient conditions are Mach number = 0·05 and static temperature (also the reference) = 294°K. The noise data are computed at far-field stations located on an

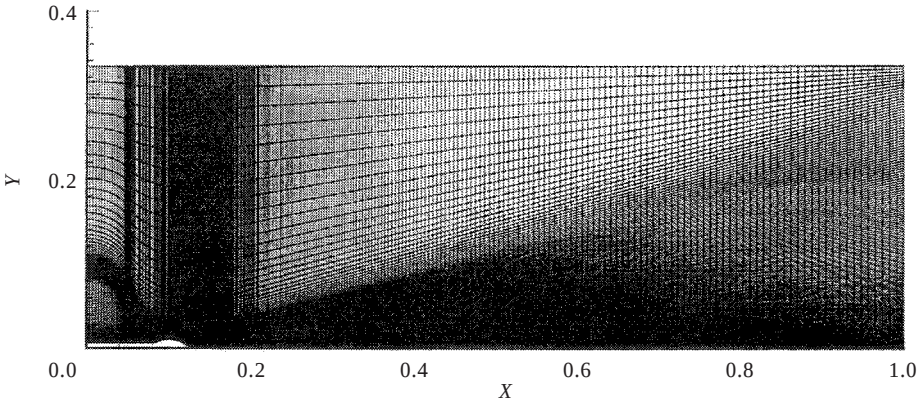

Figure 2. Grid for the CPN flow-field (aspect ratio = 3, axial length = $33D$).

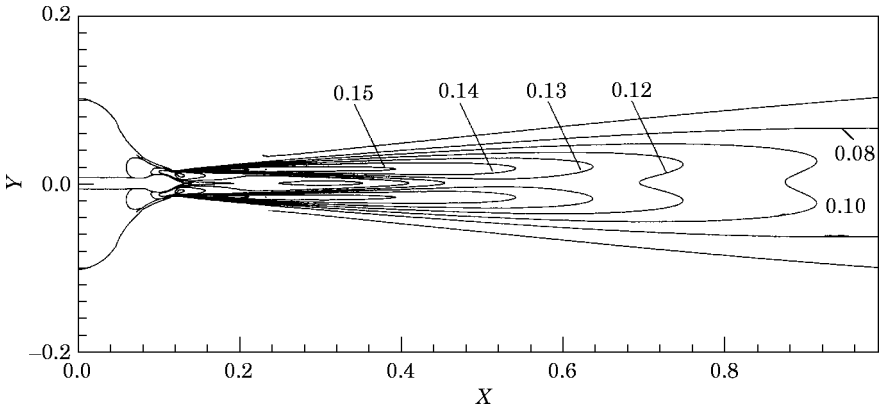

Figure 3. Contour plot of the turbulence intensity for the CPN jet ($\xi = 3{\cdot}62$: design).

arc of radius 3·05 m centered at a point on the jet axis in the exit plane of the plug-nozzle at the lip.

The gas dynamics and far-field noise of the flow field have been computed at pressure ratios $\xi = 2{\cdot}0$, 2·5, 3·0, 3·62 (design), 4·0, 4·5 and 5·0. For the first pressure ratio $\xi = 3{\cdot}62$, a run time of about five h on the Cray Y-MP supercomputer was needed to attain satisfactory convergence for the CFD computations. The result of computations at the first pressure ratio is used as the starting condition for calculations at the next adjacent pressure ratio, and the run times for subsequent computations from one adjacent pressure ratio to another are of the order of only four h. A complete set of computational acoustic data were obtained at angles, *measured from the downstream jet axis* θ, in multiples of 10° from 20°–160°.

6. RESULTS AND DISCUSSIONS

A complete set of the gas dynamics and the far-field noise data for the contoured plug-nozzle is available [24]. The available gas dynamics data consist of the predicted numerical outputs of all flow variables at the grid points along with the associated contour plots. Computational noise data include the one-third octave sound pressure levels of the mixing noise, the shock-associated noise and the total noise in the full range of the investigated pressure ratio for various angles to the jet axis. Only some typical gas dynamics and far-field noise results, which help assess the role of the CPN as a supersonic jet noise suppressor, are presented as part of the discussion that follows.

6.1. SOME GAS DYNAMIC FEATURES

Some typical contour plots of turbulence intensity and Mach number for the CPN jet flow at the design pressure ratio ($\xi_d = 3{\cdot}62$: shockless flow condition) are presented in Figures 3 and 4, respectively, and the radial distributions at selected axial locations are provided in Figure 5. The turbulence intensity level shown is normalized with respect to the acoustic speed at 294°K and is defined as $[(1/3)v_i v_i]^{1/2}/C_\infty$.

Turbulence intensity levels are noted to be very low in the entire region of the plume except in a very narrow annular region along the nozzle lip line at the free jet boundary. This is observed to be so not only for the design condition of the shockless flow, but also for all other off-design pressure ratios when shock structure is present in the jet. The thin annular region of higher turbulence intensity levels extends some twelve nozzle diameters downstream from the nozzle lip, the maximum value of the turbulence intensity level being

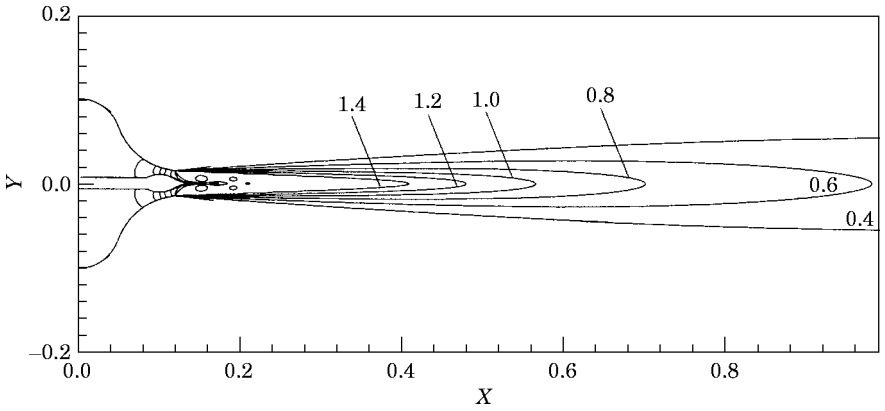

Figure 4. Contour plot of the flow-field Mach number for the CPN jet ($\xi = 3{\cdot}62$: design).

less than about 15%. The mixing region of the ideal CPN jet is thus quite narrow and is dominant only in a region near the free jet boundary adjacent to the supersonic core of the jet. The trends and magnitudes of the turbulence intensity levels of the fully-expanded (shockless) CPN jet at $\xi_d = 3{\cdot}62$ are very nearly the same as those reported in a computational study of a fully-expanded (shockless) CD nozzle jet at a *lower* design pressure ratio of $\xi_d = 3{\cdot}18$ [26].

The predicted contoured plug-nozzle jet flow at the design condition is noted to be fairly uniform at the exit plane in the vicinity of the plug tip. The supersonic core of the CPN jet at the design pressure ratio $\xi_d = 3{\cdot}62$ is noted to extend about eighteen jet diameters downstream from the plug-nozzle lip. This is significantly different from the corresponding reported value of about twelve diameters for the convergent nozzle [47] and is nearly the same as that for the CD nozzle of *lower* design pressure ratio ($\xi_d = 3{\cdot}18$) [27]. The results thus indicate that the supersonic core of the ideal CPN jet would be smaller than that of the equivalent CD nozzle jet.

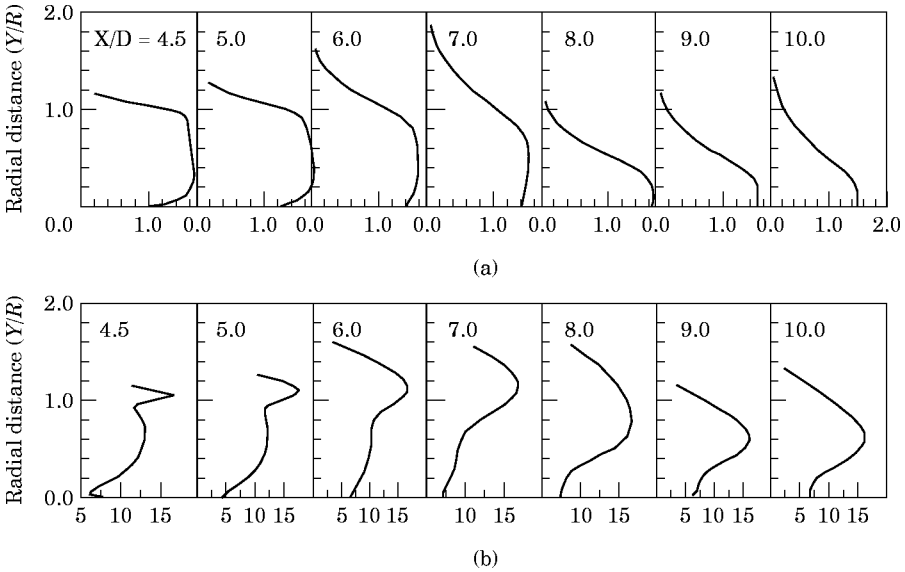

Figure 5. Radial distributions of the turbulence intensity and the Mach number at some selected axial locations for the CPN jet ($\xi = 3{\cdot}62$: design). (a) Radial Mach number profiles, (b) turbulence intensity profiles, at various axial locations.

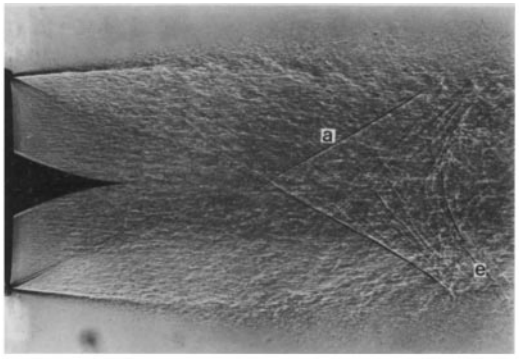

(a)

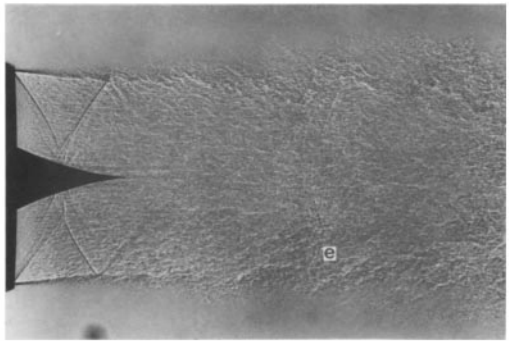

(b)

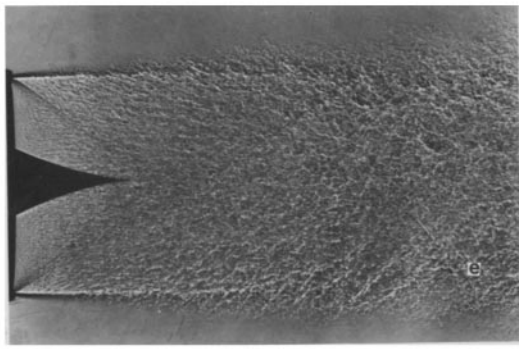

(c)

Figure 6. Typical shadowgraphs of the fully-, over- and under-expanded CPN jets: (a) $\xi = 4{\cdot}5$ (under-expanded), (b) $\xi = 2{\cdot}5$ (over-expanded), (c) $\xi = 3{\cdot}62$ (design).

The computational gas dynamics data indicate a reasonably shock free CPN jet at $\xi_d = 3{\cdot}62$. As compared to the convergent nozzle, and even convergent–divergent nozzle, relatively weak cellular shock structures are observed in the CPN jet at all off-design pressure ratios (both less than or greater than the design pressure ratio). Close to the design pressure ratio, at an imperfectly expanded jet pressure ratio $\xi = 3{\cdot}0$ or $\xi = 4{\cdot}0$, it is observed that the first few shock cells are too weak to repeat themselves farther downstream. The formations of the first shock cell in the CPN jet flows occur relatively farther downstream, and the strength of the shock cells and their extents decay rapidly.

These observations of the CPN jet flows at the design and off-desgin conditions are in general agreement with the reported shadowgraph records of the contoured plug-nozzle jet flow which are reproduced from an earlier study in Figure 6 [23]. The Mach number contour plot at the design condition of shockless flow indicates the presence of a small narrow subsonic pocket embedded in the supersonic core of the jet near its axis beyond the plug tip. This is explained by the presence of a thin separated flow region starting from the plug tip (wake flow due to a finite plug tip dimension). A similar thin wake flow is also visible in the shadowgraph of the CPN jet flow (see Figure 6 labeled as design). A significant wake flow is necessarily accompanied by a recompression shock which, if strong enough, could lead to formation of its own repetitive shock structure. An ideally pointed plug, of course, will not generate a wake but then, this is not a practical proposition. Also, the computed data exhibit no evidence of formation of wake shock or Mach disc even at the highest underexpanded jet pressure ratio ($\xi = 5{\cdot}0$) which was also found to be the case in the earlier experimental study of the CPN [15]. At such high off-design supercritical pressure ratios, the Mach disc formations always occur in the convergent and the CD nozzle jet flows.

In the present two-stage algorithm for the jet noise prediction, as mentioned earlier, the relevant CFD data are used as inputs for the noise computation. The CFD related errors would thus pass on to the prediction of the jet noise. At this stage, it is not possible to identify the sources of such errors as no experimental gas dynamics data (turbulence intensity, static pressure, velocity, Mach number, etc.) for an ideally contoured plug-nozzle jet are available in the literature to enable a satisfactory validation of the use of the NPARC code for prediction of such jet flows. In particular, the computation of the turbulence intensity which plays a key role in the generation of the mixing noise needs to be further interpreted and validated. Also, it is important to further validate the estimation of the cellular shock structure characteristics of the CPN jet flows which are responsible for generation of the often dominant shock-associated noise in imperfectly expanded jets.

6.2. MECHANISM OF SHOCK FORMATION

The operation of the CPN at a supercritical pressure ratio less than the design pressure ratio ($\xi < \xi_d$ or $M_j < M_d$) is designated here as the overexpanded mode of operation. In such flows (see the shadowgraph in Figure 6 labeled as $\xi = 2{\cdot}5$ and the sketch in Figure 7(a)), all the expansion waves between the leading wave front ($M = M_j$) and the trailing wave front ($M = 1$) of the expansion fan centered at and emanating from the nozzle lip are canceled at the contoured plug surface. However, the continued compression turning of the contoured plug surface downstream of the location, where the leading expansion wave ($M = M_j$) is incident on the plug, generates a family of compression wave fronts on their own. If the fully expanded jet flow Mach number M_j is much less than the design Mach number M_d, these compression waves generated at the plug surface may coalesce together to form a weak conical shock in the plug region close to the free jet boundary. For cases of M_j not much less than M_d, the compression waves generated by the plug surface may not coalesce to form a conical shock in the plug region. The compression fronts generated by the plug surface, or the conical shock formed by their coalescence in the plug region, reflect as expansions from the free jet boundary; these expansion waves reflect as compression waves from the opposite jet boundary; and, finally, the compression waves join together to form the first conical shock. Subsequent reflections then lead to formation of a train of weak repetitive shock cells. Because of the compression waves originating from only a part of the plug surface, such shock structure is weaker than the shock structure of an underexpanded jet flow from an equivalent convergent nozzle where the shock is formed by the coalescence of the compression waves due to reflection

of the entire expansion fan from the free jet boundary. The shock strength in such CPN flow conditions may not be strong enough to lead to the formation of repetitive shock cells. This is evident from the shadowgraph in Figure 6 labeled as $\xi = 2{\cdot}5$. The absence of a well developed train of shock cells in overexpanded ideal contoured plug-nozzle jet flows would imply considerably reduced shock-associated noise generation.

A typical shock formation in underexpanded CPN jet flows ($M_j > M_d$) is shown in Figure 7(b). The shadowgraph of such a jet flow is presented in Figure 6 labeled as $\xi = 4{\cdot}5$. In such jet flows, all of the expansion waves, corresponding to $M \leqslant M_d$, emanating from the nozzle lip are intercepted by the contoured plug surface and are canceled by the suitable compression turnings provided at the plug surface. However, some expansion waves, corresponding to $M_d < M \leqslant M_j$, escape past the plug tip, meet the free jet boundary downstream, get reflected as compression waves, and subsequently coalesce to form the first shock cell of the repetitive shock structure. Again, as in the overexpanded cases of the jet flow, only a very small portion of the waves of the expansion fan centered at the nozzle lip play a role in shock formation; and, therefore, the train of shock cells formed is relatively weak. At conditions close to the design, the first shock cell may be too weak to repeat itself. Also, the escaping expansion waves and their reflections as compression waves from the CPN jet boundary are relatively less steep, and, therefore, relative to the convergent and the CD nozzle jet flows, the first shock cell location is farther downstream and the shock cell spacing is larger. These observations are confirmed by the shadowgraphs of the underexpanded CPN jet flows of which only one has been included in Figure 6 [23].

It thus appears that the repetitive shock cell formations in contoured plug-nozzle jet flows, in both the underexpanded and overexpanded modes of operation, are relatively weak if at all present. The mechanism of shock formation in the CPN jet flow is found to be basically different from those in round convergent nozzle and convergent–divergent nozzle jet flows.

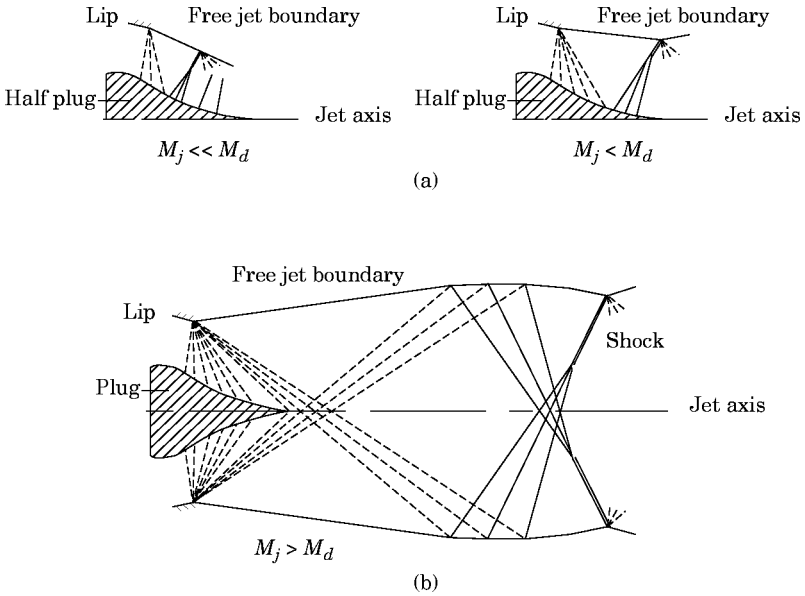

Figure 7. Shock formations in over- and under-expanded contoured plug-nozzle jets: (a) over-expanded and (b) under-expanded contoured plug-nozzle jet.

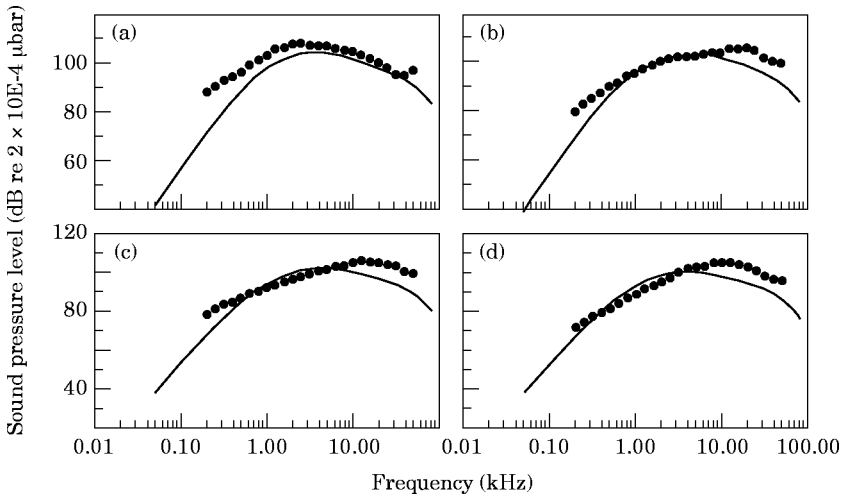

Figure 8. Comparisons of the 1/3-octave SPL spectra for the CPN jet at $\xi = 3{\cdot}62$ (design): ——, prediction; ●●●●, measurements [15]. $\theta =$: (a) 30°; (b) 60°; (c) 90°; (d) 120°.

6.3. COMPUTATIONAL NOISE PREDICTION

Some typical predicted one-third octave SPL spectra of the CPN jet flows for the full expanded ($\xi_d = 3{\cdot}62$), the overexpanded ($\xi = 2{\cdot}5$), and the underexpanded ($\xi = 4{\cdot}5$) modes of operation are compared with the experimental values [15] in Figures 8–10, respectively. Each figure shows spectra at four typical angles, *measured from the downstream jet axis*: $\theta = 30°$, 60°, 90° and 120°. The computed OASPL for the fully expanded ($\xi_d = 3{\cdot}62$), the overexpanded ($\xi = 2{\cdot}5$), and the underexpanded ($\xi = 4{\cdot}5$) modes of operation are presented in Figure 11.

6.3.1. *Noise prediction at design pressure ratio*

At the design presure ratio ($\xi_d = 3{\cdot}62$, shockless flow, Figure 8), the agreement of the predicted SPL with the measurements may be considered to be, in general, very good, the

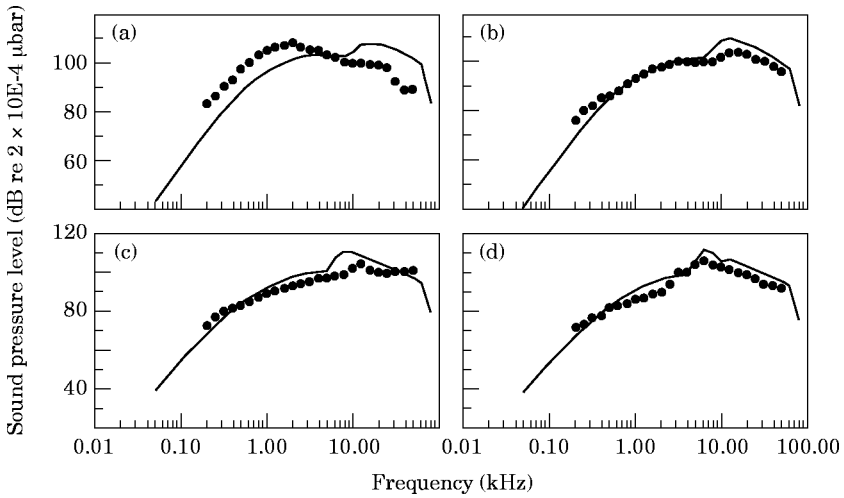

Figure 9. Comparisons of the 1/3-octave SPL spectra for the over-expanded CPN jet at $\xi = 2{\cdot}5$: ——, prediction; ●●●●, measurements [15]. $\theta =$: (a) 30°; (b) 60°; (c) 90°; (d) 120°.

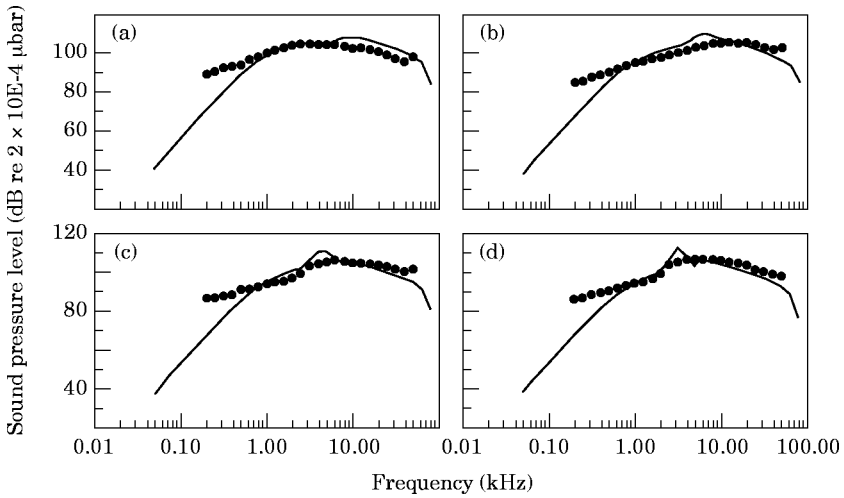

Figure 10. Comparisons of the 1/3-octave SPL spectra for the underexpanded CPN jet at $\xi = 4{\cdot}5$: ——, prediction; ●●●●, measurements [15]. $\theta =$: 30°; (b) 60°; (c) 90°; (d) 120°.

maximum deviation being of the order of 3 dB. The agreement is observed to be excellent at lower angles to the downstream jet axis in the entire range of frequencies except at their extreme values. The code slightly underpredicts the SPL generally at all angles. The deviation of predictions from measurements increases at higher angles to the jet axis, $\theta = 60°$, 90° and 120°. The maximum deviations are in the upper range of the one-third octave band center frequencies, these being up to 7 dB; outside this range of frequencies, agreement is very good. The SPL predictions at very high band center frequencies are noted to be poor at all angles to the jet axis. The computational scheme predicts a peak Strouhal number of the order of 0·3 ($f_{\text{peak}} D/U_j \cong 0{\cdot}3$), which is nearly the same at all angles. However, experimental data show that the peak Strouhal number increases with increasing angle up to 60° and then levels off to a nearly constant value. A slight shift in the predicted

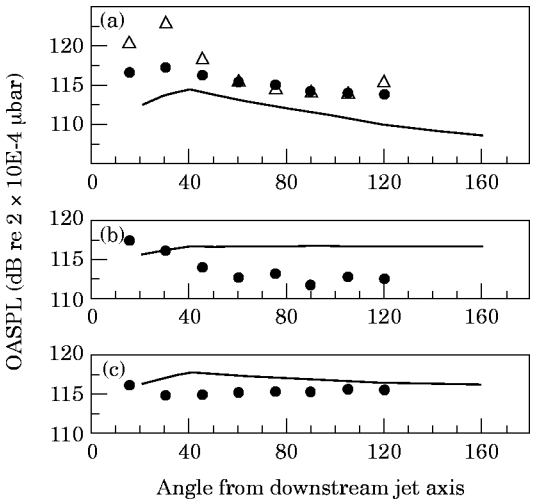

Figure 11. Comparisons of the OASPL directivity for the fully-, over- and under-expanded CPN jets: ——, prediction; ●●●●, measurements [15]; △△△△, CD nozzle [5]. $PR =$: (a) 3·62 (design: fully-expanded); (b) 2·5 (over-expanded); (c) 4·5 (under-expanded).

peak frequency to a higher value, as compared to the measurements, is observed at almost all higher angles θ. The general agreement of the one-third octave SPL predictions with the experimental data may be considered to be good though. Further, the agreement of predictions with the measurements in the present contoured plug-nozzle study is generally of the same order as that reported in an earlier computational study of the convergent–divergent nozzle [27].

The predicted variation of the OASPL versus θ for the CPN jet flow at the design pressure ratio, when the jet flow is shockless and the only noise is due to turbulent mixing, is compared with the CPN measurements in Figure 11(a). The figure also shows the experimental noise data of an equivalent CD nozzle as derived from an earlier study [5]. The agreement of the CPN computational data with the measurements are noted to be quite fair, deviations being within 3 dB in the middle range of the angle θ and slightly higher at the higher and the lower angles. The predicted maximum OASPL is noted to be about 114·5 dB at $\theta = 40^\circ$ as compared to the corresponding measurement of 117 dB at $\theta = 30^\circ$. The codes always underpredict the OASPL but the trend of variations seems to be well represented. Earlier measurements have shown that the OASPL of a contoured plug-nozzle ($M_d = 1{\cdot}49$, present case) are significantly lower than those of a contoured CD nozzle ($M_d = 1{\cdot}48$) at lower angles to the downstream jet axis [15, 5] where the mixing noise is known to be dominant. This trend is also confirmed by the present computational study. Comparisons of the present CPN OASPL versus θ prediction with a similar prediction for a CD nozzle (design pressure ratio, $\xi_d = 3{\cdot}12$) [27], when scaled down to a distance of 3·05 m (present case) based on the inverse-square law variation and when adjusted for the nozzle exit area, show the same trends. Thus, it may be concluded that the presence of a properly contoured plug may result in suppression of mixing noise also.

It appears that the combination of the NPARC CFD code and the modified GE/MGB noise code reasonably predicts the CPN jet noise at its design condition except in situations of very high frequencies and in regard to the peak Strouhal number. The computational CPN data indicate that, at the design pressure ratio, the jet flow is nearly shockless and the dominant component of the noise generation mechanism is due to mixing alone. Therefore, the reasons for the discrepancies may be traced to (a) the mixing noise modelling, and (b) the application of the code to a flow with a center-body.

The present prediction methodology assumes that the jet noise is dominated by small-scale turbulence. Until recently, it was generally believed that large-scale turbulence structures or instability waves of the flow became active as a noise source only at very high supersonic numbers. A more recent investigation of the noise spectra for both subsonic and supersonic jets indicates that both scales of turbulence structures may influence the turbulence mixing noise at all jet Mach numbers [48]. Prediction of the mixing noise due to large-scale turbulence is usually done using a linear inviscid stability analysis [49]. This noise component is dominant inside the zone of silence of fine-scale turbulence, which is formed near the downstream jet axis. It has been suggested that the dominant part of radiated noise due to large-scale turbulene is in a downstream direction for angles $\theta < 55^\circ$ with a peak Strouhal number decreasing with the angle [50]. These observations may partly explain the lack of a proper shift in the predicted spectra of the CPN at the design condition. The reason for discrepancy at very high frequencies is not very clear. It may possibly be attributed to the breakdown of modelling associated with the sound-flow interaction. Present modelling is based primarily on round jet studies which ignore the presence of a solid center-body. It appears that in plug-nozzle situations, the high-frequency solution [37, 38] may provide an adequate approximation for prediction of the jet noise over the most energetic portion of the spectrum. This issue needs to be examined further.

Errors in the mixing noise prediction may also be due to source description and propagation modelling. Validations of the source intensity formulation in the code have often reported a discrepancy of the order of 10% for simple round nozzle situations. In order to use the Lighthill's equation to predict the sound intensity, it is necessary to develop an approximate model of turbulence which will allow an analytical integration of the two-point space-time correlations. Ribner's assumption of isotropic turbulence leads to an exact analytical evaluation of the correlation volume integrals. Admittedly, the turbulence in a jet is not isotropic. For example, it has been reported that the measurements of the fourth-order velocity correlation in the direction of the flow are different from the transverse components [51]. Other models of turbulence such as axisymmetric turbulence [52] have been documented in the literature. Clearly, new computational challenges, including development of CFD codes with a non-isotropic turbulence model need to be addressed.

Several issues need to be noted in regard to the application of the present codes for predicting the jet mixing noise for plug-nozzle situations i.e., flows with center-bodies. A number of empirical parameters (α, α_c, β_c, etc.) need to be used as inputs to the codes and these parameters are to be chosen based on the available experimental data as guide. In the present study, the choice of these parameters was primarily based upon the experimental data of the convergent nozzle and the CD nozzle jet flows. No experimental data on contoured plug-nozzle jet flows are available to help determine a suitable set of values for the empirical constants. Second, the underlying mechanism of the mixing noise radiation used in the computational modelling is supported primarily by the studies on round convergent nozzle and the CDA nozzle jet flows. These studies are silent as to the effect of a center body on an otherwise free jet flow. A solid body such as a well-contoured plug immersed in an unbounded flow may influence the turbulence-related characteristics.

6.3.2. *Noise prediction at off-design pressure ratios*

Shock structures are necessarily present in supersonic jet flows at off-design conditions. The predicted noise spectra of the CPN jet flows in presence of shocks need to be examined now. The one-third octave SPL comparisons in overexpanded modes of operation, for example at $\xi = 2{\cdot}5$ (Figure 9), show a very reasonable agreement between predictions and measurements. At pressure ratios close to the design pressure ratio, the agreement is excellent in almost the entire range of frequencies at almost all angles, deviations being within 3 dB, except at very small angles when the match is rather erratic. With decreasing pressure ratio, however, the codes overpredict the SPL at very high frequencies. At the lowest pressure ratio ($\xi = 2{\cdot}0$: farthest from the design condition), where one would expect relatively pronounced repetitive shock structure in the jet flow field, excellent agreement of the predictions with measurements (within 3 dB) is noted at all angles θ except at very high frequencies where deviations are up to 10 dB. Based on examination of the detailed numerical acoustic data [24], it may be concluded that the spectra are dominated by the mixing noise at almost all angles to the jet axis at pressure ratios close to the design pressure ratio. However, at very low supercritical pressure ratios, the shock noise component is seen to dominate, in particular, at very high frequencies and at larger angles θ. For such cases, the predicted spectra for the shock-associated noise are found to be extremely broadband with the levels considerably higher than the values for the mixing noise. In fact, the predicted one-third octave band SPL for the mixing noise component are closer to the measured total noise levels [15]. Therefore, the lack of good agreement in the overexpanded modes at very high frequencies and at very low angles may be attributed to the code-related overprediction of the shock noise.

In the underexpanded modes, for example at $\xi = 4{\cdot}5$, the predictions are quite satisfactory, deviations being within 3 dB, except at very low frequencies (see Figure 10). For the very low one-third octave band center frequencies, the deviations are observed to be large, reaching values of up to 8 dB. In general, the codes underpredict the SPL in the underexpanded mode of operations whenever the deviations are significant.

Using the same codes as in this study, a computational noise prediction of a contoured CD nozzle ($\xi_d = 3{\cdot}12$) in imperfectly expanded modes of operation has been recently reported [28]. This study reported the SPL predictions to be fair except in the range of low one-third octave band center frequencies where the deviations were significant. According to this study, no noise suppression effectiveness of the CD nozzle, as compared to the equivalent underexpanded convergent nozzle, was observed at lower angles to the downstream jet axis at *any* frequency. However, significant noise suppressions of the CD nozzle were reported for high frequencies at higher angles θ where the shock associated noise is known to be a dominant component. Such is not the case for the contoured plug-nozzle of the present study where one notices noise suppression effectiveness at all pressure ratios (even at low supercritical off-design pressure ratios) for all angles to the downstream jet axis—at lower angles where the mixing noise is the dominant component as well as at higher angles where the shock-associated noise is the dominant component. It should be emphasized that the CPN experimental noise data [15] as well as the predicted noise data indicate only slight sensitivity to changes in the pressure ratio in the underexpanded mode. This may be attributed to the basically different shock formation mechanism in contoured plug-nozzle jet flow which produces only weak structures, as explained in the earlier section.

The computational OASPL versus θ variation for some typical cases, when repetitive shock structures are present in the CPN jet flows, is compared with the experimental values in Figure 11(b) for the supercritical pressure ratios less than ξ_d (overexpanded mode of operation) and in Figure 11(c) for supercritical pressure ratio greater than ξ_d (underexpanded mode of operation). In the overexpanded mode of operation (Figure 11(b)), one notices a lack of significant directivity pattern in the predicted noise radiation; the directivity pattern is noted to gradually emerge with increasing supercritical pressure ratio (being almost absent at $\xi = 2{\cdot}0$). Such a directivity pattern was not indicated in the reported measurements [15]. The trend of noise directivity as predicted by the computational study appears to be basically different at off-design supercritical pressure ratios: the measurements consistently indicate a tapering off of the OASPL from a peak at the lowest angle θ, to a gradual leveling off with increasing θ. Further, the modelling underpredicts the OASPL at smaller angles θ and overpredicts at the higher angles. Another peculiarity of the computational modelling is that it always underpredicts OASPL at lower angles θ (region of mixing noise dominance) and overpredicts at higher angles θ where the shock noise component is known to be dominant; however, the departures are reasonable, being within 5 dB.

The predictions of OASPL versus θ variations for supercritical pressure ratios, $\xi > \xi_d$ (for example, see Figure 11(c)), exhibit directivity patterns which are, again, noted to be basically different from the measurements. The predictions indicate well defined directivity pattern *always peaking at* $\theta \cong 40^\circ$, whereas the measurements indicate practically no directivity pattern in the far-field noise radiation. Further, the computational modelling underpredicts OASPL close to the design pressure ratio ξ_d and overpredicts OASPL farther away from the design pressure ratio in the entire range of the examined supercritical pressure ratios $\xi > \xi_d$, the maximum deviations being within 8 dB. Thus, the computational modelling predictions are noted to be not that satisfactory in such situations.

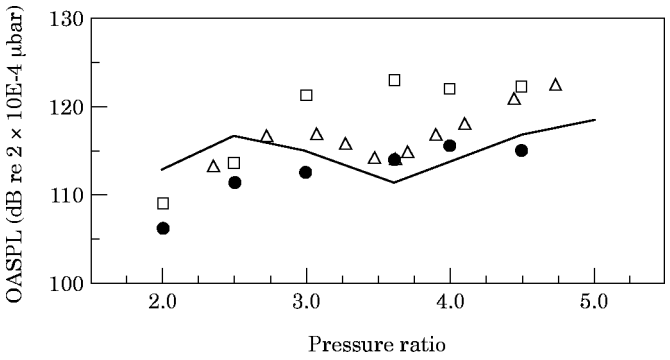

Figure 12. Comparisons of OASPL variations with pressure ratio at $\theta = 90^\circ$ for: ——, CPN prediction; ●, CPN measurements; □, equivalent convergent nozzle measurements and △, equivalent CD nozzles measurements [5].

The sources of error in the present jet noise prediction for flows with shock structures may be primarily on account of the shock-associated noise modelling and secondarily due to the mixing noise modelling problems discussed in an earlier section. As noted before, the mechanisms of shock formations in contoured plug-nozzle jet flows are basically different from those in the convergent nozzle or in the convergent–divergent nozzle jet flows. The shock-associated noise formulation of Tam and his associates incorporated in the code is based on the moderately imperfectly expanded jet flows from round convergent–divergent and convergent nozzles. Several empirical parameters such as Γ, L_w, n_1 and n_2 values for over- and underexpanded flows, etc. (see equations (12) and (15)), need to be externally prescribed for implementation of this prediction scheme. These empirical constants have been assigned values so that a better match of the prediction with the measurements for the CD nozzle and convergent nozzle jets could be attained. The same set of values has also been used in the present plug-nozzle computations as no supporting experimental data are available for the CPN jet. It may be possible to change these values arbitrarily such that one obtains a better agreement between the CPN prediction and experiment at a particular pressure ratio. Efforts to get a set of values for the empirical parameters which would work reasonably for the whole realm of either the over- or the underexpanded CPN jet flows have been unsuccessful. The shock-associated noise prediction scheme of the code is independent of the CFD of the jet flows and, being empirically based on conic nozzle data, should not be expected to predict the shock noise for a CPN nozzle. In its present state of development, the modified GE/MGB code works well only for simple nozzle geometries. In addition, one should take into consideration the effect of possible coupling of the mixing noise and the shock noise radiation which is not incorporated in the code. In order to further modify the GE/MGB code, issues related to these need to be addressed.

6.4. NOISE SUPPRESSION EFFECTIVENESS

The variation of the predicted OASPL at $\theta = 90^\circ$ with the pressure ratio ξ for the CPN jet flows is compared in Figure 12 with the experimental data for the CPN [15], the equivalent CD nozzle [5] and the equivalent convergent nozzle [15]. The contoured plug-nozzle measurements do not show the typical "bucket" pattern as exhibited by the CD nozzle. The "bucket" pattern refers to a dip in the variation of the OASP versus pressure ratio ξ for the CD nozzle at and close to the shock-free design pressure ratio ξ_d; the OASPL for the CD nozzle is 'lowest' at its design pressure ratio ξ_d (shockless flow condition) and then quickly rises to the corresponding values for the equivalent

underexpanded convergent nozzle at the off-design pressure ratios on either side of the design pressure ratio. The CPN prediction does indicate the "bucket" pattern, but this is not as pronounced as is the case for the CD nozzle. This slight appearance of the bucket is due to code-related shock-associated noise formulation as given in equation (15) which is an empirical attempt to actually *fit* the CD nozzle measurements. It is important to note that the OASPL at $\theta = 90^\circ$ for the CPN as predicted by the codes are, in general, higher than the corresponding CPN experimental values, but these values are still less than the corresponding experimental values for the equivalent CD nozzle. In addition, the predicted OASPL of the CPN are considerably lower than the values for the equivalent convergent nozzle except for very low operating pressure ratios, whereas the OASP of the equivalent CD nozzle jets at off-design pressure ratios approach those of the equivalent convergent nozzle jets. That is, the computational scheme predicts that, as a jet noise suppressor, the contoured plug-nozzle is as good as a contoured CD nozzle, if not better.

Underexpanded convergent nozzle far-field jet noise intensity is known to follow a β^4-scaling law, where $\beta = (M_j^2 - 1)^{1/2}$ is the Harper-Bourne and Fisher shock parameter [6]. A similar β^4-scaling law, where $\beta = (M_j^2 - M_d^2)^{1/2}$, is also known for the imperfectly expanded CD nozzle jet flows [12]. As opposed to the convergent nozzle and the CD nozzle, the experimental contoured plug-nozzle jet noise study [15] reported that the noise intensity varies approximately as β^2, where $\beta = (M_j^2 - M_d^2)^{1/2}$. Therefore, the rate of increase in the OASPL for the CPN is less than those for the convergent and the CD nozzles. The underlying physical reason for this is provided by the earlier observations on shock formations in the CPN jet flows; the strength of the shock structures in the CPN jet flows in the over- and underexpanded modes are relatively weaker and the shock-cell spacing relatively larger. Also, the typical phenomenon of oblique shock formation at the nozzle lip in the overexpanded CD nozzle jet flows is absent in the CPN jet flows. Consequently, the contributions of the shock-associated noise in the imperfectly expanded CPN jet flows are comparatively less. The computational data of the CPN jet noise do not indicate any β-scaling. This may be attributed to the failure of the theoretical scheme to predict the shock-associated noise at pressure ratios far removed from the design pressure ratio.

In general, the computational results well support the role of a contoured plug-nozzle as a supersonic jet noise suppressor. Further, the computational study validates the key findings of the reported experimental study [19] in regard to the noise suppression effectiveness of the contoured plug-nozzle.

7. CONCLUSIONS

Based on the results and discussions of the computational study of the ideal supersonic contoured plug-nozzle jet flows over a wide range of operating pressure ratios, some important conclusions may be drawn:

(1) The prediction of noise levels of the contoured plug-nozzle jet flow at design condition (shockless flow) is noted to be good; the model often predicts the noise levels within 3 dB. The trends as well as the magnitudes are often well represented.

(2) The modelling, in general, predicts the noise levels at off-design supercritical pressure ratios (flows with shocks) within 5 dB except at very high frequencies, when deviations up to 8 dB are observed.

(3) The role of a contoured plug-nozzle as a supersonic jet noise suppressor for low to moderate pressure ratios is well supported by the computational study.

(4) The computational noise prediction scheme consisting of a combination of the modified GE/MGB noise code and the NPARC CFD-code with k-ε turbulence modelling, is a useful engineering tool for comparative evaluations of jet noise suppression.

ACKNOWLEDGMENTS

This research was supported by NASA Lewis Research Center, Acoustics and Propulsion Branch, Cleveland, Ohio, under Grant No. NAG3-1563. A. P. Das's help in preparation of this paper is acknowledged.

REFERENCES

1. L. E. Stitt 1990 *NASA RP*-1235. Exhaust nozzles for propulsion systems with emphasis on supersonic cruise aircraft.
2. J. M. Seiner and E. A. Krejsa 1989 *American Institute of Aeronautics and Astronautics Paper* 89-2358. Supersonic jet noise and the high speed civil transport.
3. M. J. Lighthill 1962 *Philosophical Transactions of the Royal Society of London* **A267**, 147–182. The Bakerian lecture: sound generated aerodynamically.
4. A. Powell 1953 *Proceedings of the Physical Society* **66**(12B), 1039–1056. On the mechanism of choked jet noise.
5. J. C. Yu and D. S. Dosanjh 1972 *Journal of the Acoustical Society of America* **51**, 1400–1410. Noise field of a supersonic Mach 1·5 cold model jet.
6. M. Harper-Bourne and M. J. Fisher 1973 *AGARD CP*-131, 11-1 to 13. The noise from shock waves in supersonic jets, noise mechanisms, AGARD Conference on Propagation and Reduction of Jet Noise.
7. J. M. Seiner 1984 *American Institute of Aeronautics and Astronautics Paper* 84-2275. Advances in high speed jet aeroacoustics.
8. H. S. Ribner 1985 *American Institute of Aeronautics and Astronautics Journal* **43**, 1708–1715. Cylindrical sound waves generated by shock vortex interaction.
9. H. K. Tanna 1977 *Journal of Sound and Vibration* **50**, 429–444. An experimental study of jet noise, part II: shock associated noise.
10. C. K. W. Tam and H. K. Tanna 1982 *Journal of Sound and Vibration* **81**, 337–358. Shock-associated noise of supersonic jets from convergent–divergent nozzles.
11. L. Maestrello 1979 *American Institute of Aeronautics and Astronautics Paper* 79-0673. An experimental study on porous plug jet noise suppressor.
12. V. Kibens and R. W. Wlezien 1985 *American Institute of Aeronautics and Astronautics Journal* **23**, 678–684. Noise reduction mechanisms in supersonic jet with porous center-bodies.
13. K. Yamamoto, J. F. Brausch, T. F. Balsa, B. A. Janardan and P. R. Knott 1984 *NASA CR*-3845. Experimental investigation of shock-cell noise reduction for single stream nozzles in simulated flight.
14. I. S. Das and D. S. Dosanjh 1991 *Journal of Sound and Vibration* **146**, 391–406. Short conical solid/perforated plug-nozzle as supersonic jet noise suppressor.
15. D. S. Dosanjh and I. S. Das 1988 *American Institute of Aeronautics and Astronautics Journal* **6**, 924–931. Aeroacoustics of supersonic jet flows from a contoured plug-nozzle.
16. D. S. Dosanjh, P. K. Bhutiani and K. K. Ahuja 1978 *American Institute of Aeronautics and Astronautics Journal* **16**, 268–270. Jet noise suppression by co-axial cold/heated jet flows.
17. H. K. Tanna, C. K. W. Tam and W. H. Brown 1981 *NASA CR*-3454. Shock-associated noise reduction from inverted-velocity profile coannular jets.
18. J. M. Seiner and M. K. Ponton 1986 *American Institute of Aeronautics and Astronautics Paper* 86-1867. Acoustic properties associated with rectangular geometry supersonic nozzles.
19. P. J. Morris and T. R. S. Bhat 1993 *American Institute of Aeronautics and Astronautics Paper* 93-4409. Supersonic elliptic jet noise.
20. A. Khavaran and N. J. Georgiadis 1996 *American Institute of Aeronautics and Astronautics Paper* 96-0641. Aeroacoustics of supersonic elliptic jets.
21. E. A. Krejsa, B. A. Cooper, D. G. Hall and A. Khavaran 1990 *American Institute of Aeronautics and Astronautics Paper* 99-3983, *NASA TM* 103628. Noise measurements from an ejector suppressor nozzle in the NASA Lewis 9 by 15 foot low speed wind tunnel.

22. J. F. Connors and R. C. Meyer 1956 *NASA TN* 3589. Design criteria for axisymmetric and two-dimensional supersonic inlets and exits.
23. D. S. Dosanjh and I. S. Das 1987 *NASA CR*-178095. Aeroacoustics of contoured and solid/porous conical plug nozzle supersonic jet flows.
24. I. S. Das, A. Khavaran and A. P. Das 1996 *NASA CR*-198462. Computational study of a contoured plug-nozzle as a supersonic jet noise suppressor.
25. R. Mani, T. E. Balsa, P. R. Gliebe, R. A. Kantol, E. J. Stringas and J. F. C. Wang 1977 *FAA-Rd*-76-79-2. High velocity jet noise source location and reduction, task 2: theoretical developments and basic experiments.
26. H. Reichardt 1943 *Royal Aeronautical Society Journal* **47**, 167–176. On a new theory of free turbulence.
27. A. Khavaran, E. A. Krejsa and C. M. Kim 1994 *Journal of Aircraft* **31**, 603–609. Computation of supersonic jet mixing noise for an axisymmetric convergent–divergent nozzle.
28. C. M. Kim, E. A. Krejsa and A. Khavaran 1993 *American Institute of Aeronautics and Astronautics Paper* 93-0735. Computation of supersonic jet noise under imperfectly expanded conditions.
29. G. K. Cooper and J. R. Sirbaugh 1989 *Arnold Engineering Development Center Report* AEDC-TR-89-15. PARC code: theory and usage.
30. K. Y. Chien 1982 *American Institute of Aeronautics and Astronautics Journal* **20**, 33–38. Prediction of channel and boundary layer flows with a low Reynolds number turbulence.
31. R. Beam and R. F. Warming 1976 *Journal of Computational Physics* **22**, 87–110. An implicit finite difference algorithm for hyperbolic systems in conservation form.
32. B. S. Baldwin and H. Lomax 1978 *American Institute of Aeronautics and Astronautics Paper* 78-257. Thin layer approximation and algebraic model for separated turbulent flows.
33. R. Mani 1976 *Journal of Fluid Mechanics* **76**, 753–778. The influence of jet flow on jet noise, part i the noise of unheated jets.
34. R. Mani 1972 *Journal of Sound and Vibration* **25**, 337–347. Moving source problem relevant to jet noise.
35. M. E. Goldstein 1976 *Journal of Fluid Mechanics* **75**, 17–28. The low frequency sound from multipole sources in axisymmetric shear flows, part II.
36. T. F. Balsa 1977 *Journal of Fluid Mechanics* **79**, 33–47. The acoustic field of sources in shear flow with application to jet noise: convective amplification.
37. B. J. Tester and C. L. Morfey 1976 *Journal of Sound and Vibration* **46**, 79–103. Developments in jet noise modelling—theoretical predictions and comparisons with measured data.
38. S. P. Pao 1973 *Journal of Fluid Mechanics* **59**, 451. Aerodynamic noise emission from turbulent shear layers.
39. M. E. Goldstein 1976 *Aeroacoustics*. New York: McGraw-Hill Book Company.
40. H. S. Ribner 1969 *Journal of Fluid Mechanics* **38**, 1–24. Quadrupole corrections governing the pattern of jet noise.
41. J. E. Ffowcs Williams 1963 *Philosophical Transactions of the Royal Society of London* **A255**, 469–503. The noise from turbulence convected at high speed.
42. D. C. Pack 1950 *Quarterly Journal of Mechanics and Applied Mathematics* **3**, 173–181. A note on Prandtl's formula for the wavelength of a supersonic gas jet.
43. C. K. W. Tam, J. A. Jackson and J. M. Seiner 1987 *Journal of Fluid Mechanics* **153**, 123–149. A multiple scales model of the shock cell structure of imperfectly expanded supersonic jets.
44. C. K. W. Tam 1987 *Journal of Fluid Mechanics* **153**, 123–149. Stochastic model theory of broad band shock associated noise from supersonic jets.
45. C. K. W. Tam 1990 *Journal of Sound and Vibration* **140**, 55–71. Broadband shock associated noise of supersonic jets.
46. C. K. W. Tam 1989 *American Institute of Aeronautics and Astronautics Paper* 89-1088. Forward flight effects on broadband shock associated noise of supersonic jets.
47. H. T. Nagamatsu, R. F. Sheer, Jr. and G. Horva 1969 *NASA-SP*-207, 17–51. Basic Aerodynamic Research (Editor I. R. Schwartz). Supersonic jet noise theory and experiments.
48. C. K. W. Tam, M. Golebioski and M. J. Seiner 1996 *American Institute of Aeronautics and Astronautics Paper* 96-1716. On the two components of turbulence mixing noise from supersonic jets.
49. C. K. W. Tam 1991 *NASA Reference Publication* 1258, **1**, 311–390. Aerodynamics of flight vehicles: theory and practice.

50. C. K. W. TAM and P. CHEN 1994 *American Institute of Aeronautics and Astronautics Journal* **32**, 1774–1780. Turbulence mixing noise from supersonic jets.
51. I. S. F. JONES 1969 *Journal of Fluid Mechanics* **36**, 529–543. Fluctuating turbulent stresses in the noise producing region of a jet.
52. M. E. GOLDSTEIN and B. M. ROSENBAUM 1972 *NASA TN* D-6939. Emission of sound from axisymmetric turbulence convected by a mean flow with application to jet noise.

APPENDIX: NOMENCLATURE

A	area of the jet
C, C_∞	local and ambient speed of sound
f	observer frequency
I_{ijkl}	source correlation tensor
J_1	Bessel function of order one
K	annulus radius ratio of the plug-nozzle ($=R_p/R_N$)
$L_{\max}$	axial length of the plug from the sonic point to its tip
M	Mach number
p	absolute pressure
r	radial distance
R	radius (also source to observer distance)
R_P	radius of the plug at the sonic point
R_N	radius of the nozzle lip at the exit
U	mean velocity in the direction of the flow
V_i	local velocity component
v_i	fluctuating velocity component
W_t	annulus width of the throat from sonic point to the nozzle lip
y	source co-ordinate
α	inclination of the plug-nozzle lip to the jet axis
β	Harper-Bourne and Fisher parameter
γ	ratio of specific heats
ξ	ratio of reservoir absolute pressure to the ambient absolute pressure
ρ	density
ψ	wall slope of the plug at the sonic point
σ_m	mth root of the zeroth order Bessel function
θ	polar angle with respect to the downstream jet axis